

# UBR CCD photometry of Stromlo-APM galaxies

Jon Loveday\*

*Astronomy Centre, University of Sussex, Falmer, Brighton, BN1 9QJ*

17 November 2018

## ABSTRACT

We present CCD photometry in the Johnson-Kron-Cousins *UBR* bands for a sample of 320 galaxies selected from the Stromlo-APM Redshift Survey. We use this CCD data to estimate the galaxy luminosity function in the *U*, *B*, *R* and *b<sub>J</sub>* bands, finding consistent results with earlier work. Fainter galaxies serendipitously observed on our CCD frames allow a check of the photometric calibration of the APM Galaxy Survey. We find no evidence of any significant scale error in the APM magnitudes.

**Key words:** techniques: photometric — surveys — galaxies: luminosity function, mass function — cosmology: observations

## 1 INTRODUCTION

The Stromlo-APM galaxy survey (Loveday et al. 1996) — see <http://astronomy.sussex.ac.uk/~loveday/sapm> — is a sparse (1:20) sampled redshift survey containing 1797 galaxies with  $b_J < 17.15$  over a very large volume of space. The solid angle of the survey is 1.3 sr and the median redshift is about 15,300 km/s. This makes the survey very well suited to measurements of the galaxy luminosity function and large-scale clustering. Recently (Loveday 2000), we obtained near-infrared *K*-band imaging for a luminosity-selected subsample of 345 galaxies, enabling us to estimate the *K*-band (2.2 $\mu$ m) galaxy luminosity function over a range of 10 mag.

Here we present *UBR* CCD photometry for the same sample of galaxies and use this new data to estimate the galaxy luminosity function in *U*, *B*, *R* and *b<sub>J</sub>*.

The observations and data reduction are discussed in §2. We use these observations to calibrate the APM scans in §3 and present the luminosity functions in §4. We conclude in §5. Throughout, we assume a Hubble constant of  $H_0 = 100$  km/s/Mpc and an  $\Omega_M = 1, \Omega_\Lambda = 0$  cosmology in calculating distances and luminosities.

## 2 OBSERVATIONS AND DATA REDUCTION

The galaxies observed were the same sample for which we obtained *K*-band imaging (Loveday 2000). Briefly, the galaxies were selected to sample absolute  $b_J$  magnitude as uniformly as possible. In this way we were able to estimate the *K*-band luminosity function over a wide range of luminosities with a sample of modest size.

CCD imaging of the above sample of galaxies was carried out at the Cerro Tololo Interamerican Observatory (CTIO) 1.5m telescope using Tek 2048 CCD camera #5 at  $f/13.5$  (giving a pixel size of 0.24") over the ten nights 1996 September 7–16. All but the last night were photometric. Integration times of 120, 300 and 120 s were given in *U*, *B* and *R* respectively. Galaxies were observed at airmass 1–1.3; most were observed with airmass below 1.2.

The optics of the CTIO 1.5m telescope perform very poorly in the *U* band and our *U* exposures are of limited use for most galaxies. However, they were taken under photometric conditions, and so may prove potentially useful in calibrating deeper *U*-band observations taken under non-photometric conditions. Standard star sequences were observed from the compilation of Landolt (1992). Bias frames and twilight sky flats were taken at the start and end of each night.

The CCD frames were reduced within the IRAF environment. Bias frames were median filtered with minmax rejection to form a master bias for each night. The flat-field calibrations through each filter were averaged with cosmic ray rejection to form master flats for each filter for each night. Basic reduction was performed using the QUADPROC package, written at CTIO for reduction of four-amplifier CCD data. This package trims off the overscan, subtracts the bias frame, and divides by the master sky flat for the appropriate filter. Cosmic ray hits were identified and removed with the COSMICRAYS task. Finally, the *B* and *U* images of each field were aligned with the *R* image by first estimating an approximate offset with a single bright star, and then using the IMALIGN task to calculate and apply a more accurate offset. This alignment technique was also used to co-add multiple observations of a single field.

\* E-mail: J.Loveday@sussex.ac.uk

## 2.1 Image detection and photometry

We used SExtractor 2.0.15 (Bertin & Arnouts 1996) to detect and measure images in the reduced frames. In order to determine consistent colours, flux in the  $U$ ,  $B$  and  $R$  bands was measured within the same aperture for any given object. This aperture was set for each object using the  $R$  band image, since this is the most sensitive band. For image detection (but not measurement), the  $R$  band frames were convolved with a Gaussian filter of FWHM 5 pixels in order to match the typical seeing conditions of  $\approx 1.2''$ , and the detection threshold was set to 1.5 times the standard deviation of the convolved image. (For the second night of observations, 1996 Sep 08, we performed  $2 \times 2$  on-chip binning, giving a pixel size of  $0.48''$ . For this night, we smoothed with a Gaussian of FWHM 3 pixels.)

For both standard stars and galaxies, we used the MAG\_BEST estimate of magnitude. This yields a pseudo-total magnitude (Kron 1980) except in crowded fields, when a corrected isophotal magnitude is measured instead. We used SExtractor's default settings for these adaptive-aperture magnitudes, and thus measure flux inside an elliptical aperture with semi-major axis 2.5 times larger than the first moment of the light distribution. This measures roughly 94% of a galaxy's flux (Bertin & Arnouts 1996); no correction is applied for the  $\sim 6\%$  missing flux, since most other published photometry misses a similar fraction of flux.

Magnitude errors were estimated by combining in quadrature SExtractor's estimate of the error from photon statistics and the difference between magnitudes measured using local and global estimates of the sky background. Unfortunately, one of the amplifiers suffered from high read noise, making the lower-left quadrant of the CCD image of limited use. We were careful to avoid placing the target galaxy on or near this bad quadrant whilst observing, but it did mean that the global background estimate had to be estimated assuming it to be constant across the entire CCD frame. Consequently, the global background estimate is a poor approximation to the local background, and so magnitude errors are overestimated. Note that the local background estimate was used in determining galaxy magnitudes. This is unaffected by the bad quadrant.

Of the selected sample of 363 galaxies, 320 were observed under photometric conditions. Estimated magnitude errors were less than 0.5 mag for 320 observations in  $R$ , 315 in  $B$  and 189 in  $U$ .

## 2.2 Calibration

We assumed a zero-point of 25 in calculating CCD magnitudes, so that  $m = 25 - 2.5 \lg(\text{summed ADU})$ . The following transformation equations were used to convert observed CCD magnitudes  $ubr$  to  $UBR$  magnitudes on the Johnson-Kron-Cousins system:

$$\begin{aligned} R &= r + r_0 + r_X X + r_c(b - r), \\ B &= b + b_0 + b_X X + b_c(b - r), \\ U &= u + u_0 + u_X X + u_c(u - b), \end{aligned} \quad (1)$$

where  $r_0, b_0, u_0$  are the zero-point offsets,  $r_X, b_X, u_X$  the extinction coefficients multiplying the airmass  $X$ , and  $r_c, b_c, u_c$  the colour terms in the  $R, B, U$  bands respectively.

**Table 1.** Standard star extinction coefficients and magnitude residuals.

Night	$r_X$	$\sigma_r$	$b_X$	$\sigma_b$	$u_X$	$\sigma_u$
1996 Sep 07	0.019	0.041	0.204	0.035	0.308	0.149
1996 Sep 08	0.045	0.032	0.224	0.037	0.332	0.157
1996 Sep 09	0.024	0.027	0.200	0.026	0.389	0.150
1996 Sep 10	0.035	0.025	0.211	0.025	0.459	0.128
1996 Sep 11	0.037	0.030	0.246	0.028	0.411	0.135
1996 Sep 12	0.050	0.030	0.272	0.023	0.448	0.193
1996 Sep 13	0.049	0.028	0.269	0.023	0.455	0.226
1996 Sep 14	0.052	0.035	0.272	0.027	0.394	0.215
1996 Sep 15	0.053	0.022	0.259	0.022	0.356	0.200

We made a total of 282 standard star observations during the 9 photometric nights (an average of 31 per night) and we initially fitted the transformation parameters independently for each night. Averaging over nights, with equal weight per night, we obtained:

$$\begin{aligned} r_0 &= 1.821 \pm 0.010, \\ r_X &= 0.039 \pm 0.088, \\ r_c &= -0.018 \pm 0.010, \\ b_0 &= 2.124 \pm 0.074, \\ b_X &= 0.241 \pm 0.063, \\ b_c &= 0.048 \pm 0.009, \\ u_0 &= 4.781 \pm 0.624, \\ u_X &= 0.385 \pm 0.533, \\ u_c &= -0.064 \pm 0.037. \end{aligned} \quad (2)$$

Standard star observations with large residuals were omitted from the fitting procedure, most of these stars fell in the bad quadrant of the CCD. Since we expect only the extinction parameters to change from night to night, we held the zero-point and colour terms fixed as given by (2) and re-fitted the extinction terms for each night. The nightly extinction terms, along with rms residual magnitude differences from Landolt's values, are given in Table 1. Galaxy magnitudes were converted to the Johnson-Kron-Cousins system using (1) with zero-point and colour terms from (2) and extinction coefficients from Table 1. Galaxies observed during non-photometric conditions were rejected. Photometry for the target galaxies is presented in the Appendix to this paper.

## 2.3 Obtaining $b_J$ magnitudes

Couch & Newell (1980) have published a transform from  $B, R$  magnitudes to the  $B_J, R_F$  system:

$$\begin{aligned} R_F &= R - 0.058(B - R) - 0.008, \\ (B_J - R_F) &= -0.027(B - R)^2 + 1.059(B - R) - 0.017. \end{aligned} \quad (3)$$

However, as pointed out by the referee, the Couch & Newell  $B_J$  passband is rather a poor approximation to the photographic  $b_J$  band.

There are several transforms from  $B, V$  magnitudes to  $b_J$  available in the literature:

$$b_J = B - 0.23(B - V), \quad (4)$$

$$b_J = B - 0.28(B - V), \quad (5)$$

$$b_J = B - 0.275(B - V) - 0.067(B - V)^2 + 0.078. \quad (6)$$

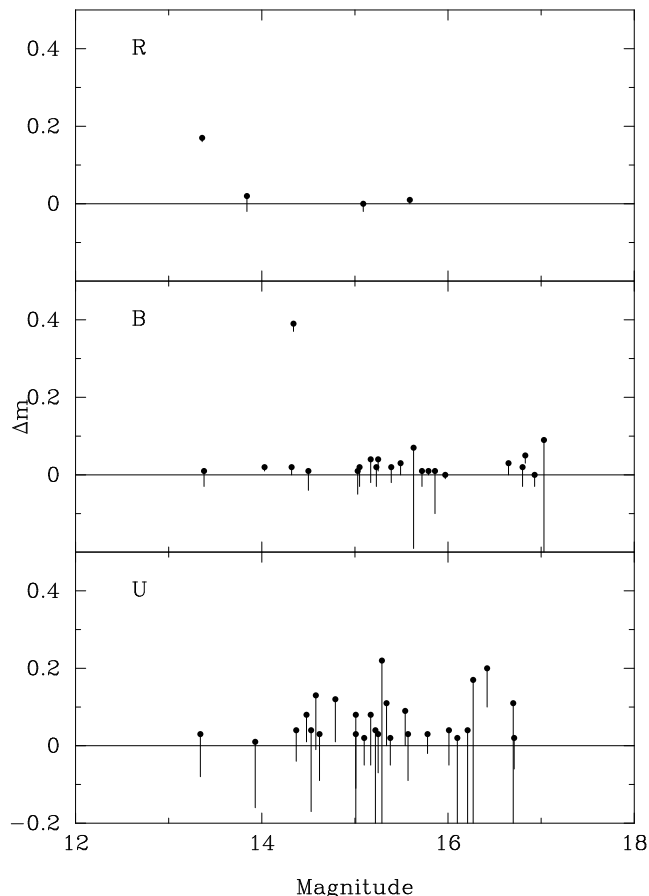


**Figure 1.** Repeatability of galaxy photometry in  $R$  (top),  $B$  (middle) and  $U$  (bottom). We plot the rms magnitude between repeated observations against the magnitude from the co-added data. The symbols indicate the rms magnitude error and the length of the line shows the estimated magnitude error.

These equations come from Kron (1978), Blair & Gilmore (1982) and Gullixson et al. (1995) respectively.

Since we do not have any  $V$  band observations, we find a relation between  $B - V$  and  $B - R$  by fitting a straight line to these colours using the standard stars of Landolt (1992). Excluding one discrepant star, we find that

$$B - V = 0.618(B - R) + 0.008, \quad (7)$$

with a scatter about this relation of 0.047 magnitudes.

Using the above, we find that the Kron, Blair & Gilmore and Gullixson et al. transforms yield consistent  $b_J$  magnitudes (with a scatter  $\sim \pm 0.02$  mag), whereas the Couch & Newell  $B_J$  magnitudes are about 0.15 mag fainter. We use the Gullixson et al. transform (6) for the rest of this paper.

## 2.4 Photometric repeatability

Thirty-one galaxies were observed on more than one occasion, mostly in  $B$  and/or  $U$ , which allows us to assess the repeatability of our photometry. In these cases, we ran SExtractor on the galaxy frames both before and after co-adding observations. We obtain final photometry from the co-added frame and use the two individual frames and the co-added frame to estimate the rms error.

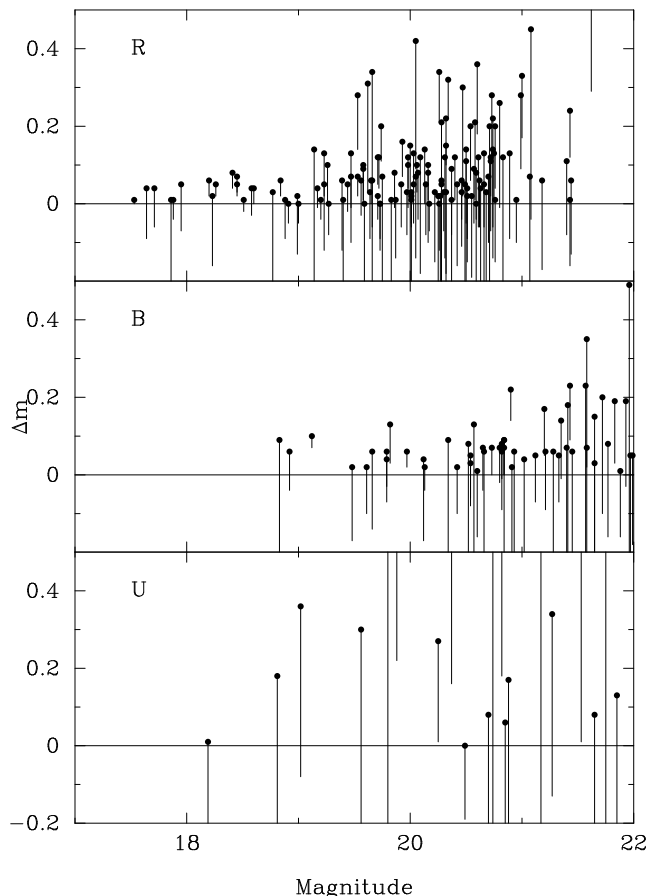


**Figure 2.** Repeatability of faint galaxy photometry in  $R$  (top),  $B$  (middle) and  $U$  (bottom). As Figure 1, but for all reliable, multiply-detected galaxies, not just target galaxies.

In Figure 1 we plot both our estimated errors and the rms errors between repeated observations as a function of magnitude for  $R$ ,  $B$  and  $U$ . The location of each symbol indicates the rms magnitude error and the length of the line shows the estimated magnitude error from the co-added image. Thus if our estimated errors are a good estimate of the true rms then the lower ends of the error bars should just reach zero. For all but one or two galaxies, the estimated error is at least as large as the rms error. The points with rms  $R$  magnitude error  $\approx 0.17$  and rms  $B$  magnitude error  $\approx 0.4$  are from the same galaxy. This galaxy is in fact one of a close pair of galaxies, and so the large discrepancy in magnitudes between the two observations presumably reflects a deblending problem. Generally however, the error is overestimated. As discussed above, this is due to the poor global background estimate. Excluding the galaxy that was poorly deblended from a close neighbour, our repeated observations lead us to estimate typical magnitude errors for our target galaxies in the  $R$ ,  $B$  and  $U$  bands of  $0.010 \pm 0.006$ ,  $0.025 \pm 0.005$  and  $0.070 \pm 0.011$  respectively.

We have also investigated the photometric reliability of fainter galaxies which by chance also lie on our CCD frames. Four of our targets were observed in all 3 bands on more than one occasion, allowing us to measure magnitude differences in each band as a function of magnitude. The results are shown in Figure 2. We see that the majority of  $R$  and  $B$

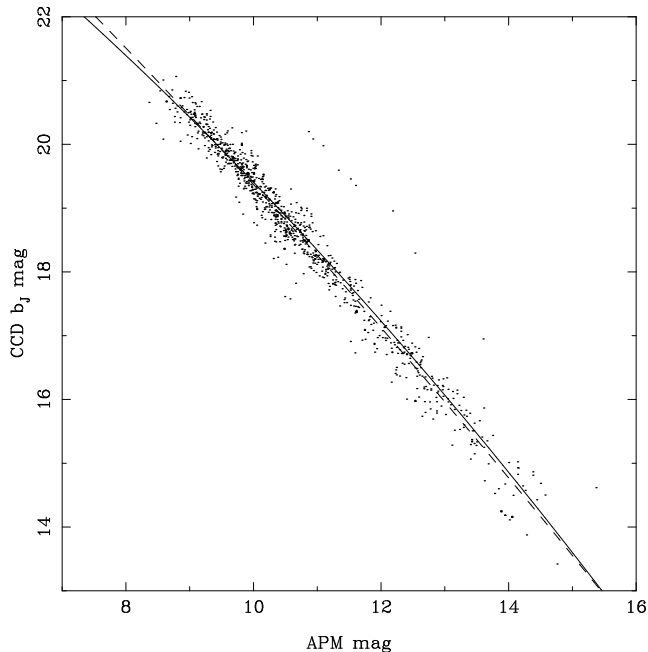


**Figure 3.** CCD  $b_J$  magnitude plotted against APM magnitude. Lines indicate quadratic functions used to convert from APM magnitudes to  $b_J$  magnitudes, allowing for photographic saturation. The continuous line shows the conversion assumed in the original APM survey (Maddox et al. 1990b) and the dashed line the best fit to our CTIO data.

magnitudes have errors  $\lesssim 0.1$  mag down to 21st magnitude. Most galaxies with a repeat error larger than this have their magnitude error set appropriately. The  $U$  band photometry, however, is very unreliable below 18th magnitude (indeed very few sources fainter than this are reliably detected in both  $U$  exposures).

We have checked that we are not systematically missing  $B$ -band flux by comparing flux measured in co-added  $B$  frames with the flux measured in individual frames. No systematic trend is seen for  $B < 22$ .

In conclusion, the  $R$  and  $B$  band photometry appears to be reliable to about 21st magnitude.  $U$  band photometry is not useful below 18th magnitude.

### 3 CALIBRATING APM SCANS

Since the CCD frames cover an area of sky around 8 arcmin on a side, they provide  $U, B, R$  photometry for many objects in each field in addition to the target galaxy. We therefore matched the images detected by SExtractor with images in the APM scans of Maddox et al. (1990c). Using the matched objects in each frame, we calculated a 6-parameter transform from CCD pixel coordinates to APM plate coordinates and thence to RA & Dec.

In Figure 3 we plot the  $b_J$  magnitude derived from our CCD data using the Gullixson et al. (1995) transform against the matched APM magnitude. This plot compares magnitudes for 1067 galaxies, ie. sources classified as non-stellar in the APM scans *and* with an SExtractor stellar likelihood `CLASS_STAR`  $< 0.5$ . We have excluded sources detected in the lower-left quadrant of the CCD due to the excessive read noise in this amplifier of the detector, all sources with

any of the SExtractor warning flags set (Bertin & Arnouts 1996), and any sources with an estimated  $b_J$  magnitude error (obtained by adding in quadrature estimated errors in  $B$  and  $R$ ) greater than 0.1 mag. All sources shown are thus expected to have “clean” CCD photometry.

The APM magnitudes have been corrected for vignetting and differential desensitisation and have been matched to be consistent from plate-to-plate, using the procedures described in Maddox et al. (1990a), but are uncorrected for photographic non-linearities and are opposite in sign from standard magnitudes, ie. a large APM magnitude implies a large flux. In Figure 3 the continuous line shows the quadratic calibration used by Maddox et al. (1990b), viz.

$$b_J = 27.405 - 0.5588m_{apm} - 0.0241m_{apm}^2, \quad (8)$$

and the dashed line shows the best fit quadratic to the present CCD data,

$$b_J = 28.984 - 0.8263m_{apm} - 0.013m_{apm}^2. \quad (9)$$

It is clear that the two calibrations agree well over the entire magnitude range plotted, although there is an overall offset of  $-0.052 \pm 0.009$  between the new and old CCD calibration, with only a very weak magnitude dependence.

There are ten outliers above and to the right of the main locus of points. These galaxy images have been visually inspected and most correspond to galaxies with close companions (either galaxies or stars), and so presumably in these cases the APM scans have blended in flux from the companion object and so have overestimated the APM magnitude.

Overall, our CCD photometry is in good agreement with the previous calibration of APM galaxies. There is no evidence for an  $\approx 20\%$  scale error in APM magnitudes as seen by Metcalfe, Fong & Shanks (1995) in one of their fields, and so presumably it is just the field in question (GSM) which suffers from this problem. Our calibrations are consistent with those recently presented by Norberg et al. (2002). The unusually steep number counts seen by Maddox et al. (1990b) are thus not explained by magnitude scale errors, but are likely to be due to a combination of large scale structure and low-redshift evolution.

### 4 LUMINOSITY FUNCTIONS

In this section we estimate luminosity functions in the  $R, B, U$  and  $b_J$  bands. Estimates of the LF in these bands over a smaller area of sky have been presented by Metcalfe et al. (1998), who used CCD calibrated photographic plates. Here we present LFs in these bands directly from CCD photometry.

In calculating rest-frame absolute magnitudes from the CCD photometry we use the  $k$ -corrections of Frei & Gunn (1994), who tabulate colours and  $k$ -corrections for four different Hubble types (E, Sbc, Scd and Im) at redshifts  $z = 0.0, 0.1, 0.2, 0.4$  and  $0.6$ . For each galaxy in our sample, we interpolate the Frei and Gunn colours to the observed redshift  $z$  and then find which of the four Hubble types provides the closest match to our observed  $(B - R)$  colour. We then use this Hubble type to estimate the  $k$ -correction in the appropriate band at redshift  $z$ .

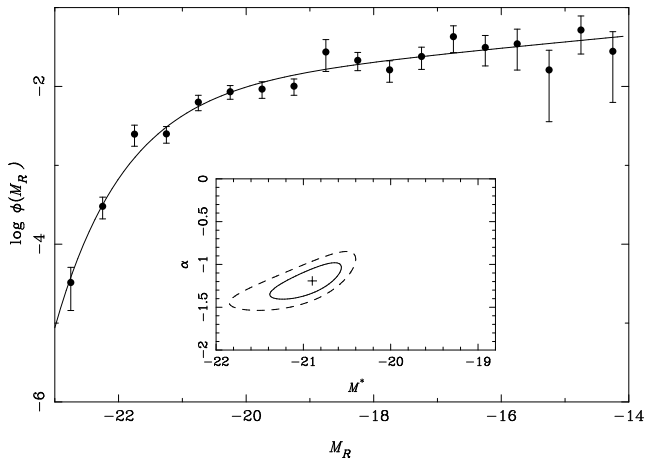


**Figure 4.** The  $R$  band luminosity function estimated from our sample (symbols) together with the best-fit Schechter function. The inset shows the 1 and 2  $\sigma$  likelihood contours for the shape parameters  $\alpha$  and  $M^*$ .

Since the sample was selected using APM  $b_J$  magnitude, it is incomplete in the CCD  $R$ ,  $B$ ,  $U$  and  $b_J$  bands. Following Loveday (2000), we estimate a bivariate luminosity function (BLF)  $\phi(M_1, M_2)$ , where  $M_1$  is the absolute magnitude inferred from the APM data and  $M_2$  is the CCD band being considered. We use a density-independent stepwise maximum likelihood (SWML) method to estimate  $\phi(M_1, M_2)$ , allowing for the known selection in  $b_J$  flux and  $M_1$  absolute magnitude. As with all density-independent estimators, information about the overall normalization is lost. We therefore normalize our BLF to the mean density of galaxies with  $-22 \leq M_1 \leq -13$  in the full Stromlo-APM sample,  $\bar{n} = 0.071 h^3 \text{Mpc}^{-3}$ , calculated as described by Loveday et al. (1992)<sup>1</sup>. We then integrate  $\phi(M_1, M_2)$  over  $M_1$  to obtain  $\phi(M_2)$ . See Loveday (2000) for full details of the procedure, which is carried out in turn using the  $R$ ,  $B$ ,  $U$  CCD magnitudes and also using a  $b_J$  magnitude inferred from the  $R$  and  $B$  magnitudes using (6) and (7).

Our estimated luminosity functions are shown in Figures 4–7. The curves show Schechter (1976) function fits to the SWML estimates using least squares, since we are unable to fit parametric models directly to incomplete data. We allow for finite bin width by calculating the mean of the predicted  $\langle \phi_j \rangle$  at the absolute magnitude of each galaxy in each bin, rather than simply calculating  $\phi(M)$  at the bin centre. The insets show 1 and 2  $\sigma$  likelihood contours for the shape parameters  $\alpha$  and  $M^*$ , where the normalization  $\phi^*$  is adjusted to maximize the likelihood at each grid point. The best-fit Schechter parameters in each band are given in Table 2, along with other estimates from the literature. The quoted errors on  $\alpha$  and  $M^*$  come from the bounding-box of the 1 $\sigma$  likelihood contours. Since our sample was  $b_J$ -selected, our galaxies tend to be fainter in the  $U$  and  $R$  bands, and so we sample the faint end of the luminosity function in these bands better than the bright end. The LF estimates were normalized to the same number density as the full Stromlo-

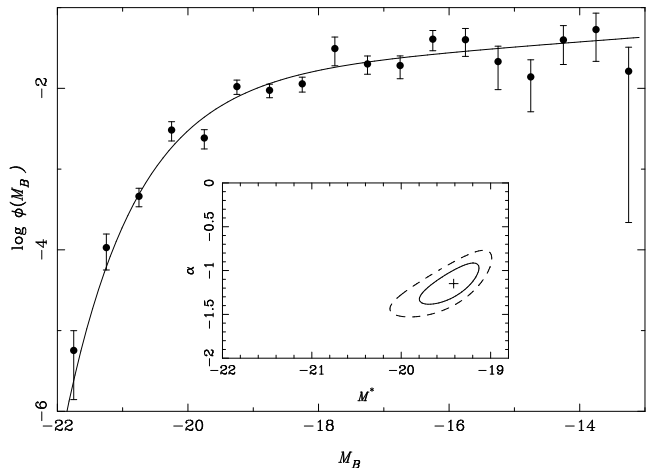


**Figure 5.** The  $B$  band luminosity function estimated from our sample (symbols) together with the best-fit Schechter function. The inset shows the 1 and 2  $\sigma$  likelihood contours for the shape parameters  $\alpha$  and  $M^*$ .

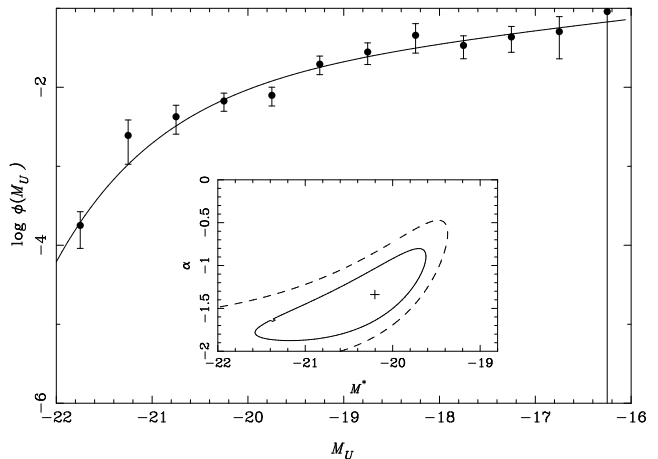


**Figure 6.** The  $U$  band luminosity function estimated from our sample (symbols) together with the best-fit Schechter function. The inset shows the 1 and 2  $\sigma$  likelihood contours for the shape parameters  $\alpha$  and  $M^*$ .

APM sample, and hence the errors in  $\phi^*$  are dominated by the uncertainty in shape of the LFs.

#### 4.1 $R$ -band luminosity function

Our estimate (Figure 4) is consistent in shape with that of Metcalfe et al. (1998), who held the faint-end slope fixed and found a characteristic magnitude rather brighter than ours, but in agreement within the quoted errors. Their  $\phi^*$  is much lower (by a factor of more than two) than other estimates shown in Table 2, reflecting the unusually low normalization of the Durham-AAT survey, eg. Ellis et al (1996).

We are also in good agreement with the LF measured in  $r^*$  from the Sloan Digital Sky Survey (SDSS, Blanton et al. 2001), albeit with considerably larger uncertainties than this much larger sample.

In agreement with the above authors, we measure a significantly steeper faint-end slope and brighter characteristic magnitude than was measured from the Las Cam-

<sup>1</sup> Note that the density  $\bar{n} = 0.047 h^3 \text{Mpc}^{-3}$  quoted by Loveday et al. (1992) is for the restricted magnitude range  $-22 \leq M_B \leq -15$ .

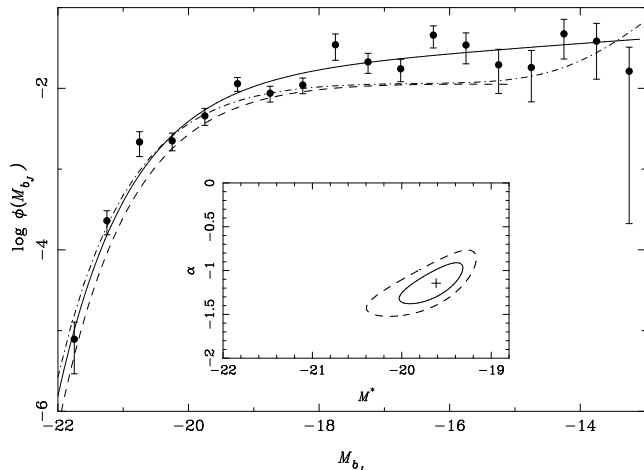


**Figure 7.** The  $b_J$  band luminosity function estimated from our sample (symbols) together with the best-fit Schechter function. The dashed line shows the Schechter function fit from Loveday et al. (1992) and the dot-dashed line the double power-law fit from Loveday (1997). The inset shows the 1 and 2  $\sigma$  likelihood contours for the shape parameters  $\alpha$  and  $M^*$ .

**Table 2.** Schechter function fits to luminosity functions.

Band	$\alpha$	$M^*$	$\phi^*(h^3\text{Mpc}^{-3})$
<b>R</b>	$-1.19 \pm 0.20$	$-20.90 \pm 0.42$	$0.014 \pm 0.011$
$R^1$	(-1.2)	$-21.24 \pm 0.10$	$0.007 \pm 0.003$
$r^{*2}$	$-1.15 \pm 0.03$	$-20.67 \pm 0.03$	$0.019 \pm 0.002$
$r^3$	$-0.70 \pm 0.05$	$-20.29 \pm 0.02$	$0.019 \pm 0.001$
<b>B</b>	$-1.15 \pm 0.25$	$-19.41 \pm 0.35$	$0.020 \pm 0.013$
$B^1$	$-1.20 \pm 0.12$	$-19.75 \pm 0.14$	$0.007 \pm 0.003$
$B^4$	$-1.12 \pm 0.05$	$-19.43 \pm 0.06$	$0.013 \pm 0.002$
<b>U</b>	$-1.34 \pm 0.55$	$-20.20 \pm 1.00$	$0.022 \pm 0.050$
$U^1$	(-1.2)	$-19.74 \pm 0.06$	$0.007 \pm 0.003$
$u^{*2}$	$-1.31 \pm 0.09$	$-18.24 \pm 0.07$	$0.047 \pm 0.011$
<b><math>b_J</math></b>	$-1.14 \pm 0.25$	$-19.62 \pm 0.35$	$0.019 \pm 0.013$
$b_J^5$	$-0.97 \pm 0.15$	$-19.50 \pm 0.13$	$0.014 \pm 0.002$
$b_J^6$	$-1.19 \pm 0.01$	$-19.79 \pm 0.04$	$0.016 \pm 0.001$

Notes: Quantities in parentheses were held fixed. Bands designated in bold face are from the present work. Other are from:

- <sup>1</sup> Metcalfe et al. (1998).
- <sup>2</sup> Blanton et al. (2001) ( $\Omega_m = 1$ ).
- <sup>3</sup> Lin et al. (1996).
- <sup>4</sup> Marzke et al. (1998).
- <sup>5</sup> Loveday et al. (1992).
- <sup>6</sup> Madgwick et al. (2002).

panas Redshift Survey (Lin et al. 1996). As discussed by Blanton et al. (2001), this difference is most likely due to the fact that Lin et al. (1996) measured isophotal magnitudes corresponding to the relatively bright isophote  $\mu_R \approx 23$  mag arcsec $^{-2}$  and that they excluded galaxies of low central surface brightness.

#### 4.2 B-band luminosity function

Our estimate (Figure 5) is in good agreement with previous measurements from the Second Southern Sky Redshift Survey (SSRS2) by Marzke et al. (1998) and by Metcalfe et al. (1998). Once again the low normalization of the Durham-AAT survey stands out.

#### 4.3 U band luminosity function

Our  $U$ -band LF is shown in Figure 6. By convolving a Schechter luminosity function with a Gaussian of width 0.07 magnitudes, we have verified that the rms magnitude error of 0.07 mag in our  $U$ -band photometry has a negligible effect on the fitted Schechter function parameters. Given the large uncertainty in our estimate of the characteristic magnitude in this band, we are consistent with Metcalfe et al. (1998). We are apparently inconsistent with the much fainter  $M^*$  found in the SDSS  $u^*$  band by Blanton et al. (2001). Note that the faint-end slope  $\alpha$  is consistent between our estimates, and so the  $\alpha$ - $M^*$  correlation is not responsible for the differing estimates of the characteristic magnitude  $M^*$ .

Part of this discrepancy can be explained by the differing response function of SDSS  $u^*$  compared with Johnson  $U$ . In order to derive an approximate conversion from Johnson  $U$  to SDSS  $u^*$ , we start with the following transform equations from Smith et al. (2002):

$$\begin{aligned} u^* - g^* &= 1.33(U - B) + 1.12, \\ g^* &= V + 0.54(B - V) - 0.07. \end{aligned}$$

Eliminating  $g^*$ ,

$$u^* = 1.33(U - B) + 0.54(B - V) + V + 1.05. \quad (10)$$

Substituting (7) into (10), we obtain

$$B - u^* = 0.29(B - R) - 1.33(U - B) - 1.05.$$

Using this equation to convert our  $UBR$  magnitudes to  $u^*$ , and fitting a straight line to  $u^*$  vs  $U$ , we find

$$u^* \approx 1.016U + 0.27, \quad (11)$$

with a scatter of 0.25 magnitudes. Our typical  $U$  magnitude of  $U \approx 16$  thus corresponds to  $u^* \approx 16.5$ , which helps to explain some, but not all, of the discrepancy between our estimate of  $M^*$  in the  $U$  band and the Blanton et al. (2001) estimate of  $M^*$  in the SDSS  $u^*$  band.

The discrepancy might be further reduced by the fact that the  $U$  response is slightly bluer than  $u^*$ . Thus the most luminous galaxies in  $U$ , which dominate our  $M^*$  estimate and which will be intrinsically blue in a  $b_J$ -selected survey, will be systematically fainter in  $u^*$ . This effect is not accounted for in our simple conversion from  $U$  to  $u^*$  (11).

#### 4.4 $b_J$ luminosity function

Our estimate (Figure 7) agrees well with that measured using APM magnitudes from the full Stromlo-APM survey (Loveday et al. 1992), although there is evidence for a slightly steeper faint-end slope  $\alpha$  in the present result. Our estimate of the characteristic magnitude  $M^*$  is also slightly brighter. This is due to the use of the Gullixson et al. (1995)  $b_J$  transform used here, whereas Loveday et al. (1992) used the Couch & Newell (1980) transform, which yields  $B_J$  magnitudes fainter by about 0.15 mag.

From the 2dF Galaxy Redshift Survey, Madgwick et al. (2002) find a slightly brighter characteristic magnitude than our result. This is likely to be due to the significantly deeper mean redshift of the 2dF survey compared with the Stromlo-APM survey. We are not able to probe far enough down the faint end of the LF to confirm or refute the upturn in the LF around  $b_J \approx -14$  claimed by Loveday (1997).

5 CONCLUSIONS

We have presented CCD photometry in the Johnson-Kron-Cousins *UBR* bands for a sample of 320 galaxies selected from the Stromlo-APM Redshift Survey. We have derived  $b_J$  magnitudes from this data in order to check the calibration of the APM scans. We find no evidence for a significant scale error in the APM magnitudes, in agreement with Norberg et al. (2002), but contrary to the findings of Metcalfe, Fong & Shanks (1995). It thus appears likely that the apparent scale error found by Metcalfe et al. was due to a single bad field.

We have measured the galaxy luminosity function in the *U*, *B*, *R* and  $b_J$  bands. The *U*-band LF is consistent with the previous determination from calibrated photographic plates by Metcalfe et al. (1998), but inconsistent with the  $u^*$  LF measured from the Sloan Digital Sky Survey (Blanton et al. 2001). The discrepancy is lessened, however, once the difference between Johnson *U* and SDSS  $u^*$  bands is allowed for. The *B*, *R* and  $b_J$  band LFs are also consistent with previous determinations, in particular with the  $b_J$  luminosity function determined from photographic magnitudes in the full Stromlo-APM survey (Loveday et al. 1992).

The original aims of this project included estimating bivariate luminosity functions and subdividing the sample by restframe *U* – *R* colour in order to compare with Canada France Redshift Survey (CFRS) observations (Lilly et al. 1995) at higher redshifts and so to constrain galaxy evolution models. The limited depth of our *U* band data precludes the latter, and has now been superseded by the Sloan Digital Sky Survey (SDSS, York et al. 2000), which has already obtained high quality five-colour photometry for hundreds of thousands of galaxies. We plan to make use of SDSS data for such investigations.

ACKNOWLEDGMENTS

It is a pleasure to thank the CTIO staff for their excellent support, Simon Lilly for sharing the observing, Steve Maddox and Nigel Metcalfe for useful discussions and the referee for a very constructive report.

REFERENCES

Bertin, E. & Arnouts, S., 1996, *A&AS*, 117, 393  
 Blair, M. & Gilmore, G., 1982, *PASP*, 94, 742  
 Blanton M., et al., 2001, *AJ*, 121, 2358  
 Couch, W.J. & Newell, E.B., 1980, *PASP*, 92, 746  
 Ellis, R.S., Colless, M., Broadhurst, T., Heyl, J., Glazebrook, K., 1996, *MNRAS*, 280, 235  
 Frei Z., Gunn J.E., 1994, *AJ*, 108, 1476  
 Gullixson, C.A., Boeshaar, P.C., Tyson, J.A., Seitzer, P., 1995, *ApJS*, 99, 281  
 Kron, R.G., 1978, PhD Thesis, Univ. California, Berkeley  
 Kron, R.G., 1980, *ApJS*, 43, 305  
 Landolt, A.U., 1992, *AJ*, 104, 340  
 Lilly, S.J. et al. 1995, *ApJ*, 455, 108  
 Lin, H., Kirshner, R. P., Sheckman, S.A., Landy, S.D., Oemler, A. , Tucker, D.L. & Schechter, P.L., 1996, *ApJ*, 464, 60  
 Loveday, J., 1996, *MNRAS*, 278, 1025

Loveday, J., 1997, *ApJ*, 489, 29  
 Loveday, J., 2000, *MNRAS*, 312, 557  
 Loveday, J., Peterson, B.A., Efstathiou, G. & Maddox, S.J., 1992, *ApJ*, 390, 338  
 Loveday, J., Peterson, B.A., Maddox, S.J., & Efstathiou, G., 1996, *ApJS*, 107, 201  
 Maddox, S.J., Efstathiou, G. & Sutherland, W.J., 1990a, *MNRAS*, 246, 433  
 Maddox, S.J., Sutherland, W.J. Efstathiou, G., Loveday, J. & Peterson, B.A., 1990b, *MNRAS*, 247, 1P  
 Maddox, S.J., Sutherland, W.J. Efstathiou, G., & Loveday, J., 1990c, *MNRAS*, 243, 692  
 Madgwick D., et al., 2002, *MNRAS*, 333, 133  
 Marzke, R.O., da Costa, L.N., Pellegrini, P.S., Willmer, C.N.A. & Geller, M.J., 1998, *ApJ*, 503, 617  
 Metcalfe, N., Fong, R. & Shanks, T., 1995, *MNRAS*, 274, 769  
 Metcalfe, N., Ratcliffe, A., Shanks, T., Fong, R., 1998, *MNRAS*, 294, 147  
 Norberg P., et al., 2002, *MNRAS*, 336, 907  
 Schechter, P.L., 1976, *ApJ*, 203, 297  
 Smith J.A., et al, 2002, *AJ*, 123, 2121  
 York D.G., et al., 2000, *AJ*, 120, 1579

APPENDIX A: THE CCD DATA

In Table A1 we present a sampling of our CCD data (42 galaxies out of a total of 320). We have included galaxies even with very large ( $\gtrsim 1$  mag) colour errors; the user may wish to treat these as non-detections. The complete catalogue will be available from the Vizier Catalogue Service (<http://vizier.u-strasbg.fr/>). The first five columns of this table come from the Stromlo-APM survey (Loveday et al. 1996). The subsequent seven columns are derived from our new observations. Each column in the table is described below.

- (1) Name: Galaxy naming follows the same convention as the APM Bright Galaxy Catalogue (Loveday 1996) and the Stromlo-APM Redshift Survey (Loveday et al. 1996).
- (2), (3) RA, dec: Right ascension (hours, minutes, seconds) and declination (degrees, arcminutes, arcseconds) in 1950 coordinates.
- (4)  $b_J$ :  $b_J$  magnitude.
- (5)  $cz$ : Heliocentric recession velocity in km/s.
- (6) *R*: *R* magnitude and its estimated error.
- (7) *B* – *R*: *B* – *R* colour and its estimated error.
- (8) *U* – *B*: *U* – *B* colour and its estimated error.
- (9), (10) Maj, Min: Semi-major and minor axes of measurement ellipse in arcseconds.
- (11) PA: Position angle in degrees measured clockwise from south-north line.
- (12) Flags: Flags output by SExtractor (Bertin & Arnouts 1996).

**Table A1.** CCD galaxy photometry.

Name	RA	Dec	$b_J$	$cz$	$R$	$B - R$	$U - B$	Maj	Min	PA	Flags
075+069-077	21 26 16.37	-68 39 53.3	16.32	11033	15.09 ± 0.04	1.49 ± 0.08	0.27 ± 0.18	19	12	52	2
076-113-015	22 56 20.64	-69 43 06.6	16.48	3813	15.63 ± 0.18	1.03 ± 0.24	-0.94 ± 0.22	32	14	60	0
077+055+032	23 11 33.04	-70 38 10.8	17.05	33310	16.44 ± 0.01	-1.44 ± 0.01	-0.73 ± 0.06	16	9	116	3
077+062-116	23 11 36.12	-67 52 12.9	16.57	29923	14.89 ± 0.04	-0.94 ± 0.09	0.00 ± 0.00	28	22	159	3
078-130-118	00 21 06.17	-62 46 46.8	16.52	12128	16.43 ± 0.01	0.47 ± 0.01	-3.93 ± 0.11	15	9	107	3
078+012+091	23 57 37.39	-66 47 31.6	15.42	21754	14.00 ± 0.14	1.86 ± 0.18	-0.77 ± 0.21	28	25	66	2
078+109+066	23 39 46.85	-66 14 01.5	14.62	10150	13.61 ± 0.01	0.99 ± 0.02	0.00 ± 0.00	48	21	84	3
080-018-033	01 31 33.11	-64 28 28.6	17.01	8088	16.42 ± 0.33	1.05 ± 0.49	-0.66 ± 0.75	17	14	127	0
080+009+024	01 26 43.01	-65 31 49.0	14.84	1624	13.68 ± 0.02	1.08 ± 0.02	-0.73 ± 0.02	26	21	14	0
082+032-078	02 50 37.37	-63 38 30.4	16.68	30356	15.73 ± 0.03	1.29 ± 0.06	-0.16 ± 0.45	22	9	102	0
107-053-114	21 24 40.36	-62 56 09.3	17.09	8507	16.23 ± 0.02	0.89 ± 0.10	-0.67 ± 0.21	24	8	152	0
108+093+006	21 43 24.76	-65 10 25.7	16.03	10497	15.29 ± 0.01	0.95 ± 0.07	-0.42 ± 0.17	21	14	38	0
108-114+028	22 20 24.21	-65 32 46.0	16.63	6146	15.77 ± 0.09	0.97 ± 0.18	0.00 ± 0.00	28	16	99	0
108-105+055	22 19 19.57	-66 03 24.1	14.56	10779	13.58 ± 0.05	1.25 ± 0.06	0.00 ± 0.00	54	22	49	2
108-083-130	22 13 20.13	-62 38 40.3	16.85	36934	15.66 ± 0.14	1.41 ± 0.17	-1.15 ± 0.54	17	15	131	0
109+063+033	22 32 40.84	-65 41 37.3	16.69	21798	14.91 ± 0.02	1.84 ± 0.07	0.00 ± 0.00	19	15	128	0
109+014+028	22 41 34.01	-65 37 16.2	14.84	3269	14.02 ± 0.03	1.16 ± 0.04	-0.71 ± 0.08	26	26	63	2
110+020+024	23 24 18.95	-65 32 45.2	15.04	1991	13.23 ± 0.06	0.88 ± 0.07	-1.37 ± 0.11	79	48	164	2
111+063-007	23 50 48.93	-59 58 26.5	14.81	3320	14.12 ± 0.02	0.94 ± 0.04	-0.54 ± 0.14	37	17	32	0
111+118+005	23 42 33.53	-60 08 39.0	15.52	3414	14.90 ± 0.10	0.96 ± 0.11	-0.69 ± 0.13	65	15	72	0
111+025+058	23 56 29.36	-61 11 27.6	16.20	28872	15.14 ± 0.05	1.76 ± 0.14	0.00 ± 0.00	28	16	173	2
112+092-034	00 24 46.45	-59 24 30.9	15.97	11668	14.71 ± 0.09	1.34 ± 0.09	-0.18 ± 0.26	23	17	77	0
112-083-068	00 50 12.34	-58 47 36.5	16.15	5150	19.43 ± 0.15	-1.02 ± 0.60	-0.62 ± 1.13	5	4	88	3
112+079+009	00 26 25.33	-60 13 13.5	16.62	4720	18.72 ± 0.07	1.56 ± 0.14	0.09 ± 0.55	3	3	17	0
113+004+088	01 15 15.04	-61 43 42.3	15.31	8591	14.16 ± 0.01	1.31 ± 0.01	-0.45 ± 0.08	34	12	6	2
114-031+009	01 58 39.99	-60 14 34.1	17.06	6743	15.85 ± 0.07	1.28 ± 0.09	-0.63 ± 0.33	25	8	122	0
114-015+074	01 56 18.04	-61 27 21.5	14.80	7002	12.52 ± 0.05	1.38 ± 0.05	-0.29 ± 0.15	64	48	108	0
114-123-003	02 12 22.81	-59 56 14.5	16.35	1471	15.95 ± 0.28	0.74 ± 0.32	-0.36 ± 0.25	57	11	99	2
116-048-060	03 17 06.64	-58 58 03.9	16.62	21466	15.38 ± 0.05	1.24 ± 0.05	-0.38 ± 0.19	14	13	89	0
117+080-131	03 36 49.50	-57 36 19.7	16.02	4952	14.73 ± 0.01	1.24 ± 0.01	-0.43 ± 0.09	23	8	30	0
117+097-087	03 34 07.28	-58 24 46.6	16.11	17774	15.19 ± 0.08	1.09 ± 0.10	-0.62 ± 0.24	23	10	96	0
144+044-118	20 47 21.43	-57 52 35.6	15.32	3233	14.44 ± 0.13	1.09 ± 0.17	-0.52 ± 2.25	35	26	164	0
144-126-031	21 12 03.18	-59 26 26.9	16.24	9493	14.63 ± 0.08	1.33 ± 0.13	0.00 ± 0.00	17	15	139	0
144+095-133	20 40 26.42	-57 34 32.3	16.93	10964	15.27 ± 0.01	1.56 ± 0.02	-0.41 ± 0.10	16	11	129	0
144+091+082	20 39 21.60	-61 34 36.5	15.69	22306	14.66 ± 0.34	1.65 ± 0.45	0.00 ± 0.00	36	25	87	2
145+055+050	21 23 44.04	-61 02 29.3	15.32	4404	12.96 ± 0.01	1.07 ± 0.01	-3.01 ± 0.01	38	12	80	3
145-099-026	21 46 53.28	-59 35 26.3	16.36	8053	14.77 ± 0.10	1.60 ± 0.14	-0.25 ± 0.66	20	15	53	0
145+035+005	21 26 58.51	-60 13 18.9	15.07	8660	13.19 ± 0.12	1.35 ± 0.18	-0.75 ± 0.22	54	40	129	2
147-070+099	22 59 03.11	-61 53 25.3	17.02	7787	16.25 ± 0.36	1.04 ± 0.38	-1.43 ± 0.69	24	17	93	2
148+099-068	23 11 40.26	-58 46 11.3	16.55	3376	15.48 ± 0.03	0.71 ± 0.03	0.00 ± 0.00	20	11	24	0
149-013-101	00 01 43.21	-53 11 47.1	14.60	9773	12.86 ± 0.07	1.68 ± 0.12	0.00 ± 0.00	38	30	167	0
149+031+040	23 55 51.03	-55 48 43.0	16.27	9477	14.78 ± 0.01	1.51 ± 0.01	-0.22 ± 0.06	27	7	9	0